Applied Physics Letters ARTICLE scitation.org/journal/apl

Thermal imaging of anomalous Ettingshausen effect at low temperatures using infrared lock-in thermography

Cite as: Appl. Phys. Lett. XX
Submitted: May 2025
Published Online: XX

Takumi Imamura,[1,2] Takamasa Hirai,[2,a)] Weinan Zhou,[2] Yuya Sakuraba,[1,2] and Ken-ichi Uchida[1,2,3,a)]

AFFILIATIONS

[1]Graduate School of Science and Technology, University of Tsukuba, Tsukuba, Ibaraki 305-8573, Japan
[2]National Institute for Materials Science, Tsukuba, Ibaraki 305-0047, Japan
[3]Department of Advanced Materials Science, Graduate School of Frontier Sciences, The University of Tokyo, Kashiwa, Chiba 277-8561, Japan

[a)]**Authors to whom correspondence should be addressed**: HIRAI.Takamasa@nims.go.jp; UCHIDA.Kenichi@nims.go.jp

ABSTRACT

Thermal imaging technology has significantly advanced the fields of thermal engineering and fundamental physics by providing precise and non-contact temperature measurements. In the field of spin caloritronics, an active infrared emission microscopy based on the lock-in thermography (LIT) has greatly developed thermoelectric and thermal transport physics in magnetic materials and their hybrid structures, but measurements have been limited to at or above room temperature. Here, we report on the measurements of transverse thermoelectric conversion in a magnetic material, the anomalous Ettingshausen effect (AEE), below room temperature using the LIT technique. Although the infrared emission decreases with decreasing temperature, LIT with the high temperature resolution allows to observe the AEE-induced temperature modulation in a ferromagnetic Heusler alloy Co_2MnGa slab down to 200 K and reliably quantify the anomalous Nernst coefficient down to around 240 K. The methodology demonstrated in this work will pave the way for further developments in both fundamental research and practical applications in spin caloritronics.

Spin caloritronics is an interdisciplinary field of spintronics and thermal energy engineering and deals with transport phenomena and cross-correlations encompassing electron charge, spin, and heat.[1–4] This research field was sparked by the discovery of the spin Seebeck effect (SSE) in 2008. SSE refers to the generation of a spin current by applying a temperature gradient to a magnetic material, resulting in an unconventional functionality of thermoelectric conversion that is completely different from the Seebeck effect.[5,6] Efforts on early spin caloritronics studies focused on thermally-induced spin transports by extending electrical measurement methods used in spintronics. In contrast, the observation of the spin Peltier effect (SPE),[7,8] the Onsager reciprocal of SSE: a temperature modulation as a result of a spin current injection into magnetic materials, caused a stir in this field about 10 years ago. One of the methods that supported to obtain SPE is the lock-in thermography (LIT),[8] in which a combination of non-contact thermal imaging through an infrared camera and lock-in detection technique enables highly sensitive temperature measurements with a temperature resolution of <1 mK.[9] LIT revealed different length and energy scales of thermally and electrically excited spin currents, which contribute to SSE and SPE, respectively, uncovering a physical mechanism that is not just in the simple Onsager reciprocal relation.[10] LIT has contributed not only to observation of various unconventional thermoelectric

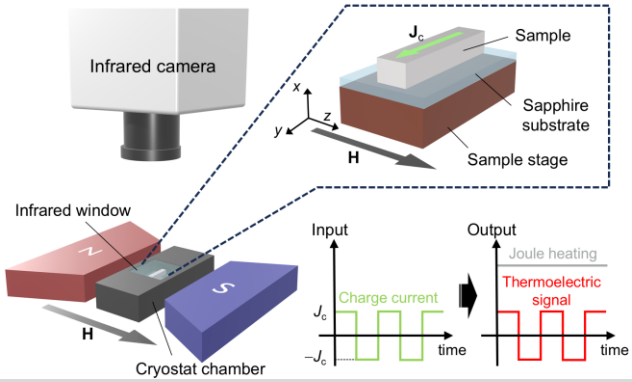

FIG. 1. Schematic of the thermographic measurement configuration. The sample temperature T was controlled by liquid N_2 flow and a heater attached to the stage. Thermal images were monitored by an infrared camera through an infrared-transparent CaF_2 window. When performing lock-in thermography (LIT) measurements, an ac square-wave-modulated charge current $\mathbf{J}_c$ and magnetic field $\mathbf{H}$ were applied to the sample.

cooling/heating[11–15] and thermal transport[16–18] appearing in the presence of a magnetic field and/or magnetization of magnetic materials, but also to quantification of other thermal energy engineering properties.[19–26]

Although the thermographic imaging technique has developed both physics and next-generation thermal management technology, most of the measurements via infrared cameras have been performed at or above room temperature. This is due to the well-known Stefan-Boltzmann law, describing that the intensity of infrared emission decays in proportion to the fourth power of the black body's temperature, which will dramatically reduce the sensitivity of thermal imaging. Furthermore, there are no reports of LIT measurements below room temperature, and it is not yet clear at what temperature range the high-temperature resolution provided by LIT is quantitatively maintained.

In this study, we have validated the availability of the LIT technique for measurements of spin-caloritronic phenomena at low temperatures. Here, we focus on measuring the anomalous Ettingshausen effect (AEE),[27–29] a transverse magneto-thermoelectric effect in magnetic materials, which generates a heat current in the direction of the cross product of an input charge current and spontaneous magnetization. Its Onsager reciprocal, the anomalous Nernst effect (ANE), is one of the most vigorously studied phenomena alongside SSE/SPE in recent spin caloritronics and topological materials science for both physics and device applications.[30–38] As a target material for measuring AEE using LIT, we selected a polycrystalline Co_2MnGa (CMG) Heusler alloy, which has developed a large transverse thermopower, i.e., anomalous Nernst coefficient S_{ANE} comparable to or even larger than that of single crystalline CMG.[38–46] By developing the LIT system for low temperature measurements and calibrating the infrared intensity, we ensure the AEE signal in CMG down to about 200 K. The temperature dependence of S_{ANE} estimated by the LIT technique shows the consistent trend with that obtained by the conventional thermoelectric measurement down to 240 K, confirming the validity of LIT for spin caloritronics even at low temperatures.

The polycrystalline CMG alloy was prepared by a spark plasma sintering technique (the detailed recipe and procedure for sample preparation are described in Ref. 38). First, Co, Mn, and Ga shots were arc-melted in an Ar atmosphere, then the CMG ingot was homogenized in high vacuum at 1000°C. Subsequently, the ingot was crushed using a mortar and planetary ball mill, followed by sieving a powder. Finally, the CMG powder was sintered at 850°C and a pressure of 30 MPa for 60 min under the vacuum condition.

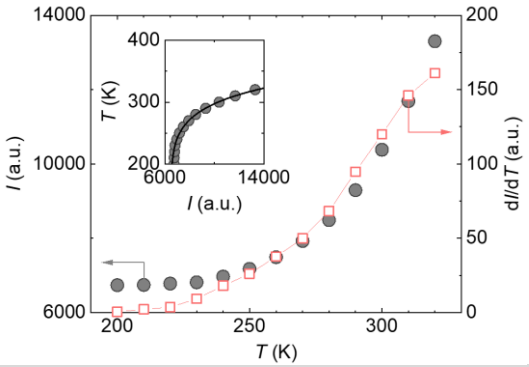

FIG. 2. Sample temperature T dependence of the intensity of infrared emission I and the sensitivity of our LIT system dI/dT. Inset shows curve fitting results for estimating dI/dT. The fitting function is $T = a(I-b)^c$ with fitting parameters a, b, and c ($0<c<1$).

Figure 1 shows a schematic of set-up for thermographic measurements in this study. The sample was installed in a custom-made sample-in-vacuum liquid N_2 cryostat. The CMG slab with a dimension of 0.7 (x) × 10.0 (y) × 3.1 (z) mm was fixed on a sapphire substrate mounted on a Cu stage, in which a heater and resistance temperature sensor were embedded, and the stage temperature was controlled by a temperature controller (Lakeshore 336). Here, the high thermal conductivity of sapphire substrate thermally stabilizes the stage and CMG slab, enabling precise measurements of temperature dependence of thermal responses. The infrared intensity of the sample surface in a high vacuum ($<10^{-4}$ Pa) was monitored by an infrared camera with an InSb quantum detector (installed in Enhanced Lock-in Thermal Emission: ELITE, DCG Systems G.K.)

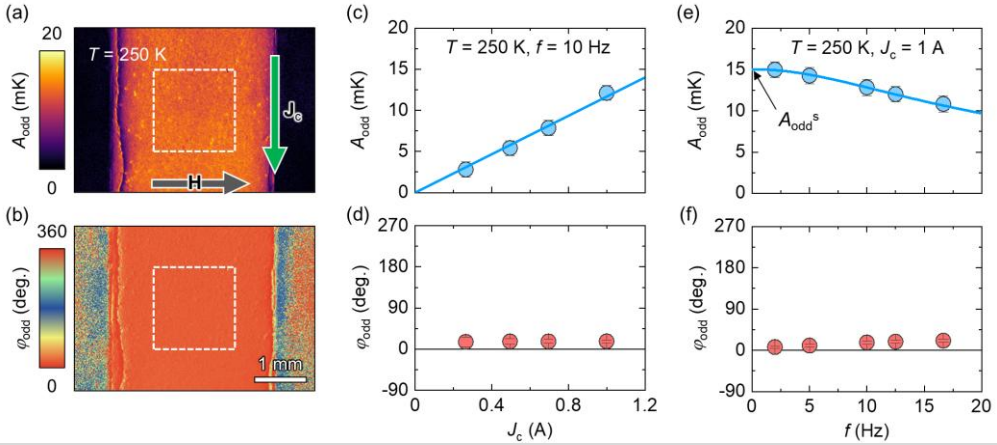

FIG. 3. Magnetic-field-odd (H-odd) component of lock-in amplitude (A_{odd}) (a) and phase (φ_{odd}) (b) images at T = 250 K, lock-in frequency f = 10 Hz, amplitude of ac square-wave-modulated charge current J_c = 1 A, and $\mu_0|H|$ = 400 mT, where μ_0 is the vacuum permeability. J_c dependence of the A_{odd} (c) and φ_{odd} (d) values at T = 250 K and f = 10 Hz. f dependence of the A_{odd} (e) and φ_{odd} (f) values at T = 250 K and J_c = 1 A. The data points are obtained by averaging the A_{odd} and φ_{odd} signals on the areas defined by the dashed square in (a) and (b), respectively. The error bars represent the standard deviation of the data in the corresponding squares. Solid line in (c) and curve in (e) show the fitting result based on a linear function and one-dimensional heat diffusion equation, respectively.

through an infrared-transparent CaF_2 window with the size of 12 × 12 mm, where the InSb detector was cooled by a Stierling cooler to 77 K. The viewing area of thermal images was 3.15 × 4.65 mm. To ensure the infrared emissivity, the surface of the slab was coated with insulating black ink.

First, to calibrate the conversion coefficient between the sample temperature T and the intensity of infrared emission I detected through our infrared camera, we measured I at the surface of the CMG slab by changing T (Fig. 2). Here, the T value was assumed to be the same as the stage temperature because we waited for a long time (>15 min) to determine T after the sensor value got stabilized at the target temperature. With the decrease in T, the I value was rapidly reduced, following to the Stefan-Boltzmann law, and the change in I with respect to T also slows down. Note that the finite I signal around 200 K is dominantly due to parasitic signals coming from the inside of the infrared camera and lens and does not affect the sensitivity of LIT. By estimating the T dependence of the sensitivity of LIT, dI/dT, it was found that the dI/dT value became zero around 200 K. The magnitude of dI/dT at 200 K was 0.04% of that at 300 K. Thus, we concluded that the lower limit for LIT measurements in this configuration is around 200 K. Note that, the increase in the dI/dT value appears to be saturated at 320 K. This suggests that the high-temperature measurement limit of the InSb detector at high temperature is approaching. This can be resolved by changing the integration time of infrared emission, but since high-temperature measurements have been extensively studied in previous research, we will exclude this from the scope of this study.

Based on these results, we performed the LIT measurements of AEE in the CMG slab at various T values below 310 K (see supplementary material S1 for detailed configuration of LIT). During the LIT measurements, an ac square-wave-modulated charge current $\mathbf{J}_c$ with the frequency f, amplitude J_c, and zero dc offset was applied to the slab along the y axis, where by extracting first harmonic response of thermal images, the thermoelectric contributions ($\propto J_c$) can be separately extracted from Joule-heating contribution ($\propto J_c^2$: constant in time for such a $\mathbf{J}_c$ condition; see also Fig. 1). The detected infrared images were converted into lock-in amplitude A and phase φ images via Fourier analysis, in which the A image shows the magnitude of temperature modulation and the φ image the sign as well as the time delay of the temperature modulation due to the thermal diffusion. Here, when converting the infrared emission to the temperature for A signals at each T, the slope of curve fitting in the inset of Fig. 2 was used. Since the AEE-induced temperature modulation shows the magnetic-field-odd (H-odd) dependence, the complex calculation of $A_{odd} = |A(+H)e^{-\varphi(+H)} - A(-H)e^{-\varphi(-H)}|/2$ and $\varphi_{odd} = -\arg[A(+H)e^{-\varphi(+H)} - A(-H)e^{-\varphi(-H)}|/2]$ with the $A(+H)$ [$A(-H)$] and $\varphi(+H)$ [$\varphi(-H)$] images measured with applying a positive (negative) magnetic field $\mathbf{H}$ along the $+z$ ($-z$) axis can extract the AEE contribution free from the Peltier effect. In this configuration, a heat flow originating from AEE occurs in the x axis, resulting in a uniform temperature change on the sample surface,[47] which allows to quantify the anomalous Nernst coefficient independently of thermal boundary conditions between the slab and stage. Figures 3(a) and 3(b) respectively present a result of the low-T LIT measurements: A_{odd} and φ_{odd} images at $T = 250$ K, $f = 10$ Hz, $J_c = 1$ A, and $\mu_0|H| = 400$ mT, where μ_0 is the vacuum permeability. Note that the value of 400 mT is sufficient for saturating the magnetization of the CMG slab in the z axis at 200–310 K (see supplementary material S2) and the contribution of the ordinary Ettingshausen effect at 400 mT is negligibly small in the CMG slab.[38] The uniform A_{odd} and φ_{odd} signals was shown in the sample region. The φ_{odd} value of approximately 0°, i.e., the heating signal, under the direction of $\mathbf{J}_c$ and $\mathbf{H}$ shown in Fig. 3(a) corresponds to the positive anomalous Ettingshausen coefficient ($= S_{ANE}T$), which is consistent with the sign of S_{ANE} of CMG.[38–46] Figure 3(c) [3(d)] shows the J_c dependence of the A_{odd} (φ_{odd}) values, where A_{odd} has a linear relationship and φ_{odd} is constant with respect to J_c. Figure 3(e) [3(f)] shows the f dependence of the A_{odd} (φ_{odd}) values. With decreasing f, that is, approaching the thermal steady state, A_{odd} increases slightly and φ_{odd} gets closer to 0°. These behaviors obtained below room temperature are consistent with the AEE-induced heat current and its thermal diffusion in the CMG slab with mm-scale dimensions.

Next, we take a look at the T dependence. Figure 4(a) [4(b)] shows the A_{odd} (φ_{odd}) images at $f = 2$ Hz, $J_c = 1$ A, $\mu_0|H| = 400$ mT, and $T = 230$, 270, and 310 K. Although the A_{odd} signal gradually decreases with decreasing T due to the reduced sensitivity, the uniform φ_{odd} signal independent of T is shown in the three images [see also Figs. 4(c) and 4(d)], indicating that the AEE-induced heat current along the x axis is clearly confirmed by ~230 K. On the other hand, below 230 K, as the T value gets closer to 200 K, the AEE signal can be detected, but the uniformness of the φ_{odd} signal dramatically gets worse and the A_{odd} signal becomes vanishingly small (see supplementary material S3). Therefore, in the quantitative discussion that follows, we will focus on data above 230 K.

Finally, we evaluated the S_{ANE} value using the equation of $S_{ANE} = \pi A_{odd}^s \kappa / 2 j_c t T$,[48,49] where A_{odd}^s, κ, j_c, and t are the AEE signal

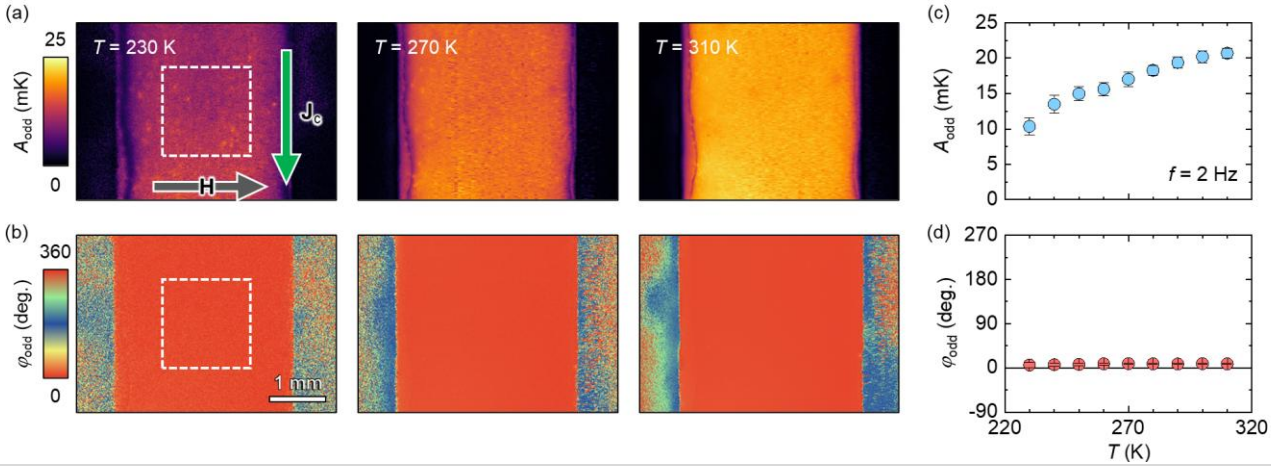

FIG. 4. A_{odd} (a) and φ_{odd} (b) images at $f = 2$ Hz, $J_c = 1$ A, $\mu_0|H| = 400$ mT, and $T = 230$, 270, and 310 K. T dependence of the A_{odd} (c) and φ_{odd} (d) values at $f = 2$ Hz and $J_c = 1$ A. The data points are obtained by averaging the A_{odd} and φ_{odd} signals on the areas defined by the dashed square in the left most panels of (a) and (b), respectively.

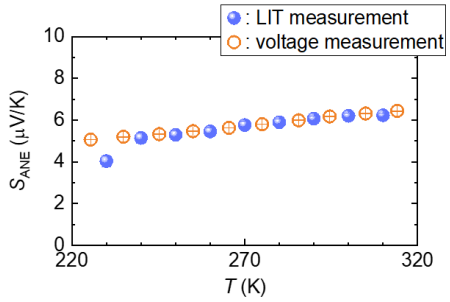

FIG. 5. *T* dependence of the anomalous Nernst coefficient S_{ANE} estimated by LIT and conventional thermoelectric voltage measurement methods.

amplitude in the steady state, i.e., at $f \to 0$ Hz, thermal conductivity, amplitude of charge current density, and sample length along the x axis (= 0.7 mm), respectively (see also supplementary material S4). From the T dependence of A_{odd}s estimated by fitting the f dependence of A_{odd} [Fig. 3(e)] with the solution of the one-dimensional heat diffusion equation in the frequency domain[48] and κ measured by the laser flash, differential scanning calorimetry, and Archimedes method in combination (see supplementary material S5), we estimated the T dependence of S_{ANE} as shown in Fig. 5. Note that the well-fitted result in Fig. 3(e) also shows that the CMG slab is in a nearly adiabatic condition in the current f range at each temperature. At 300 K, the S_{ANE} value is estimated to be 6.2 μV/K, which is comparable to that of single-crystalline bulk CMG[39,41] as previous studies have reported.[38,43,45] The T dependence of S_{ANE}, the slight decrease with decreasing T, and the S_{ANE} value at 230 K of 4.0 μV/K also show similar trend to those in previous reports (S_{ANE} = 4−5 μV/K in Sakai et al.[39] and 4 μV/K in Guin et al.[41] for single crystalline CMG and 4 μV/K in Chen et al.[45] for polycrystalline CMG at ~230 K). However, the steep decrease in S_{ANE} around 230−240 K also occurs, which was not reported in previous studies. Therefore, to confirm the validity of our low-T LIT measurements, we quantitatively compared with the conventional method of measuring ANE: measurements of a transverse thermoelectric voltage by applying a temperature gradient to the sample using the Physical Property Measurement System (PPMS-VersaLab, Quantum Design Inc.) and nanovoltmeter (2182A, Keithley). The results of the voltage measurements are also summarized in Fig. 5. Both results are in good agreement, but the steep decrease in the S_{ANE} value around 230 K is not shown, suggesting that the quantitative reliability of our LIT method is assured down to around 240 K.

In conclusion, we have demonstrated the LIT-based thermal imaging of a spin-caloritronic phenomenon, AEE, below room temperature. We observed the AEE-induced temperature modulation from 310 K to 200 K and revealed the quantitative reliability of the method down to 240 K. Although the value of 240 K is not that low in recent cryogenic research field, there are a number of magnetic materials with their Curie temperature between room temperature to ~200 K, such as ultrathin 3*d* transition metal films,[50,51] magnetic semiconductors,[52,53] layered topological materials and van der Waals heterostructures,[37,54–57] exhibiting unconventional static and transport properties. One way to extend the temperature range to lower temperatures is to use a different infrared detector. Although InSb is the most commonly used infrared detector in LIT, increasing attention has been directed toward far-infrared-compatible approaches, including HgCdTe-based detectors and quantum well infrared photodetectors. As the temperature of samples decreases, the peak wavelength of the infrared emission shifts toward longer wavelengths. Thus, employing these detectors could potentially allow for LIT measurement at lower temperature than that shown in this study. LIT has a distinct advantage at high-throughput material exploration using chemically composition-spread materials[58,59] and spatial-resolved elucidation of non-uniform thermal transport/conversion in artificial-structured composites materials[38,60,61] in spin caloritronics, compared with conventional electrical measurements. Our report on the low-temperature LIT method and analysis is versatile even for such materials, experiments, and other spin-caloritronic phenomena [SPE,[7,8] the anisotropic magneto-Peltier effect,[11] the (anisotropic) magneto-Thomson effect,[12,15] the transverse Thomson effect,[62] etc; some of them exhibit unconventional behavior that cannot be predicted from electrical measurements based on the Onsager reciprocal relation], which will aid in developing thermal and thermoelectric transport physics as well as spintronic thermal management technology at low temperature.

See supplementary material for more information about the saturation field of the CMG slab at low temperature, LIT results at T = 200−230 K, and T dependence of κ.

The authors thank R. Iguchi, F. Ando, S. J. Park, A. Ray, R. Toyama, N. Kojima, H. Yanagihara, and T. Yagi for technical supports and valuable discussions. This work was partially supported by ERATO "Magnetic Thermal Management Materials Project" (No. JPMJER2201) from JST, Japan; Grant-in-Aid for Research Activity Start-up (No. 22K20495) and Grant-in-Aid for Scientific Research (S) (No. 22H04965) from JSPS KAKENHI, Japan; and NEC Corporation.

DATA AVAILABILITY

The data that support the findings of this study are available from the corresponding author upon reasonable request.

REFERENCES

[1] G. E. W. Bauer, E. Saitoh, and B. J. van Wees, Nat. Mater. **11**, 391 (2012).
[2] S. R. Boona, R. C. Myers, and J. P. Heremans, Energy Environ. Sci. **7**, 885 (2014).
[3] K. Uchida, Proc. Jpn. Acad., Ser. B **97**, 69 (2021).
[4] K. Uchida and R. Iguchi, J. Phys. Soc. Japan **90**, 122001 (2021).
[5] K. Uchida, S. Takahashi, K. Harii, J. Ieda, W. Koshibae, K. Ando, S. Maekawa, and E. Saitoh, Nature **455**, 778 (2008).
[6] K. Uchida, J. Xiao, H. Adachi, J. Ohe, S. Takahashi, J. Ieda, T. Ota, Y. Kajiwara, H. Umezawa, H. Kawai, G. E. W. Bauer, S. Maekawa, and E. Saitoh, Nat. Mater. **9**, 894 (2010).
[7] J. Flipse, F. K. Dejene, D. Wagenaar, G. E. W. Bauer, J. Ben Youssef, and B.J. van Wees, Phys. Rev. Lett. **113**, 027601 (2014).
[8] S. Daimon, R. Iguchi, T. Hioki, E. Saitoh, and K. Uchida, Nat. Commun. **7**, 13754 (2016).
[9] O. Breitenstein, W. Warta, and M. Langenkamp, *Lock-in Thermography: Basics and Use for Evaluating Electronic Devices and Materials* (Springer, Berlin/Heidelberg, Germany 2010).
[10] A. Takahagi, T. Hirai, R. Iguchi, K. Nakagawara, H. Nagano, and K. Uchida, Appl. Phys. Express **15**, 063002 (2022).
[11] K. Uchida, S. Daimon, R. Iguchi, and E. Saitoh, Nature **558**, 95 (2018).
[12] K. Uchida, M. Murata, A. Miura, and R. Iguchi, Phys. Rev. Lett. **125**, 106601 (2020).
[13] T. Hirai, H. Sepehri-Amin, K. Hasegawa, T. Koyama, R. Iguchi, T. Ohkubo, D. Chiba, and K. Uchida, Appl. Phys. Lett. **118**, 022403 (2021).
[14] R. Modak, M. Murata, D. Hou, A. Miura, R. Iguchi, B. Xu, R. Guo, J. Shiomi, Y. Sakuraba, and K. Uchida, Appl. Phys. Rev. **9**, (2022).
[15] R. Modak, T. Hirai, S. Mitani, and K. Uchida, Phys. Rev. Lett. **131**, 206701 (2023).
[16] K. Tomioka, K. Uchida, R. Iguchi, and H. Nagano, J. Appl. Phys. **128**, 215103 (2020).
[17] Y. Kainuma, R. Iguchi, D. Prananto, V. I. Vasyuchka, B. Hillebrands, T.

An, and K. Uchida, Appl. Phys. Lett. **118**, (2021).
[18] T. Imamura, T. Hirai, K. Oyanagi, R. Iguchi, K. Takamori, S. Kobayashi, and K. Uchida, Phys. Rev. Appl. **23**, 024018 (2025).
[19] Y. Hirayama, R. Iguchi, X.F. Miao, K. Hono, and K. Uchida, Appl. Phys. Lett. **111**, 163901 (2017).
[20] H. Nakajima, T. Morimoto, Y. Okigawa, T. Yamada, Y. Ikuta, K. Kawahara, H. Ago, and T. Okazaki, Sci. Adv. **5**, eaau3407 (2019).
[21] T. Ishizaki, T. Igami, and H. Nagano, Rev. Sci. Instrum. **91**, (2020).
[22] D. Morelli, R. Marani, E. D'Accardi, D. Palumbo, U. Galietti, and T. D'Orazio, IEEE Trans. Instrum. Meas. **70**, 2515214 (2021).
[23] T. Hirai, R. Iguchi, A. Miura, and K. Uchida, Adv. Funct. Mater. **32**, 2201116 (2022).
[24] R. Iguchi, D. Fukuda, J. Kano, T. Teranishi, and K. Uchida, Appl. Phys. Lett. **122**, 082903 (2023).
[25] J. Rittmann and M. Kreutzbruck, Sci. Rep. **13**, 17093 (2023).
[26] P. Liu, A. Alasli, L. Wang, and H. Nagano, Appl. Therm. Eng. **255**, 123929 (2024).
[27] T. Seki, R. Iguchi, K. Takanashi, and K. Uchida, Appl. Phys. Lett. **112**, 152403 (2018).
[28] J. Wang, Y. K. Takahashi, and K. Uchida, Nat. Commun. **11**, 2 (2020).
[29] P. Wang, W. Xia, J. Shen, Y. Chen, W. Peng, J. Zhang, H. Pan, X. Yu, Z. Liu, Y. Gao, Q. Niu, Z. Xu, H. Yang, Y. Guo, and D. Hou, Natl. Sci. Rev. **11**, nwad308 (2024).
[30] T. Miyasato, N. Abe, T. Fujii, A. Asamitsu, S. Onoda, Y. Onose, N. Nagaosa, and Y. Tokura, Phys. Rev. Lett. **99**, 086602 (2007).
[31] Y. Sakuraba, Scr. Mater. **111**, 29 (2016).
[32] M. Ikhlas, T. Tomita, T. Koretsune, M. T. Suzuki, D. Nishio-Hamane, R. Arita, Y. Otani, and S. Nakatsuji, Nat. Phys. **13**, 1085 (2017).
[33] K. Uchida, W. Zhou, and Y. Sakuraba, Appl. Phys. Lett. **118**, 140504 (2021).
[34] T. Asaba, V. Ivanov, S. M. Thomas, S. Y. Savrasov, J. D. Thompson, E. D. Bauer, and F. Ronning, Sci. Adv. **7**, eabf1467 (2021).
[35] Y. Pan, C. Le, B. He, S. J. Watzman, M. Yao, J. Gooth, J. P. Heremans, Y. Sun, and C. Felser, Nat. Mater. **21**, 203 (2022).
[36] F. Ando, T. Hirai, and K. Uchida, APL Energy **2**, 016103 (2024).
[37] S. Noguchi, K. Fujiwara, Y. Yanagi, M. Suzuki, T. Hirai, T. Seki, K. Uchida, and A. Tsukazaki, Nat. Phys. **20**, 254 (2024).
[38] T. Hirai, F. Ando, H. Sepehri-Amin, and K. Uchida, Nat. Commun. **15**, 9643 (2024).
[39] A. Sakai, Y. P. Mizuta, A. A. Nugroho, R. Sihombing, T. Koretsune, M. T. Suzuki, N. Takemori, R. Ishii, D. Nishio-Hamane, R. Arita, P. Goswami, and S. Nakatsuji, Nat. Phys. **14**, 1119 (2018).
[40] H. Reichlova, R. Schlitz, S. Beckert, P. Swekis, A. Markou, Y. C. Chen, D. Kriegner, S. Fabretti, G. Hyeon Park, A. Niemann, S. Sudheendra, A. Thomas, K. Nielsch, C. Felser, and S. T. B. Goennenwein, Appl. Phys. Lett. **113**, 212405 (2018).
[41] S. N. Guin, K. Manna, J. Noky, S.J. Watzman, C. Fu, N. Kumar, W. Schnelle, C. Shekhar, Y. Sun, J. Gooth, and C. Felser, NPG Asia Mater. **11**, 16 (2019).
[42] K. Sumida, Y. Sakuraba, K. Masuda, T. Kono, M. Kakoki, K. Goto, W. Zhou, K. Miyamoto, Y. Miura, T. Okuda, and A. Kimura, Commun. Mater. **1**, 89 (2020).
[43] W. Zhou, A. Miura, T. Hirai, Y. Sakuraba, and K. Uchida, Appl. Phys. Lett. **122**, 062402 (2023).
[44] R. Uesugi, T. Higo, and S. Nakatsuji, Appl. Phys. Lett. **123**, 252401 (2023).
[45] M. Chen, J. Wang, K. Liu, W. Fan, Y. Sun, C. Felser, and T. Zhu, Adv. Energy Mater. **14**, 2400411 (2024).
[46] K. Oyanagi, H. Sepehri-Amin, K. Takamori, T. Tadano, T. Imamura, R. Nagasawa, K. Mahalingam, T. Hirai, F. Ando, Y. Sakuraba, S. Kobayashi, and K. Uchida, Acta Mater. **296**, 121239 (2025).
[47] R. Das, R. Iguchi, and K. Uchida, Phys. Rev. Appl. **11**, 034022 (2019).
[48] A. Miura, H. Sepehri-Amin, K. Masuda, H. Tsuchiura, Y. Miura, R. Iguchi, Y. Sakuraba, J. Shiomi, K. Hono, and K. Uchida, Appl. Phys. Lett. **115**, 222403 (2019).
[49] A. Miura, K. Masuda, T. Hirai, R. Iguchi, T. Seki, Y. Miura, H. Tsuchiura, K. Takanashi, and K. Uchida, Appl. Phys. Lett. **117**, 082408 (2020).
[50] D. Chiba, S. Fukami, K. Shimamura, N. Ishiwata, K. Kobayashi, and T. Ono, Nat. Mater. **10**, 853 (2011).
[51] A. Obinata, Y. Hibino, D. Hayakawa, T. Koyama, K. Miwa, S. Ono, and D. Chiba, Sci. Rep. **5**, 14303 (2015).
[52] Y. Yamada, K. Ueno, T. Fukumura, H.T. Yuan, H. Shimotani, Y. Iwasa, L. Gu, S. Tsukimoto, Y. Ikuhara, and M. Kawasaki, Science **332**, 1065 (2011).
[53] L. Chen, X. Yang, F. Yang, J. Zhao, J. Misuraca, P. Xiong, and S. Von Molnár, Nano Lett. **11**, 2584 (2011).
[54] Y. Deng, Y. Yu, Y. Song, J. Zhang, N. Z. Wang, Z. Sun, Y. Yi, Y. Z. Wu, S. Wu, J. Zhu, J. Wang, X. H. Chen, and Y. Zhang, Nature **563**, 94 (2018).
[55] X. J. Dong, J. Y. You, Z. Zhang, B. Gu, and G. Su, Phys. Rev. B **102**, 144443 (2020).
[56] I. A. Verzhbitskiy, H. Kurebayashi, H. Cheng, J. Zhou, S. Khan, Y. P. Feng, and G. Eda, Nat. Electron. **3**, 460 (2020).
[57] H. Zheng, C. Huang, F. Lin, J. Fan, H. Liu, L. Zhang, C. Ma, C. Wang, Y. Zhu, and H. Yang, Appl. Phys. Lett. **122**, 023103 (2023).
[58] H. Masuda, R. Modak, T. Seki, K. Uchida, T.-C. Lau, Y. Sakuraba, R. Iguchi, and K. Takanashi, Commun. Mater. **1**, 75 (2020).
[59] R. Modak, T. Hirai, Y. Sakuraba, S. Mitani, K. Oyanagi, T. Yamazaki, T. Seki, and K. Uchida, Adv. Phys. Res. **3**, 2400021 (2024).
[60] K. Uchida, T. Hirai, F. Ando, and H. Sepehri-Amin, Adv. Energy Mater. **14**, 2302375 (2024).
[61] F. Ando, T. Hirai, A. Alasli, H. Sepehri-Amin, Y. Iwasaki, H. Nagano, and K. Uchida, Energy Environ. Sci. **18**, 4068 (2025).
[62] A. Takahagi, T. Hirai, A. Alasli, S.J. Park, H. Nagano, and K. Uchida, Nat. Phys. (2025); doi: 10.1038/s41567-025-02936-3.